

# Towards Ground Truth Evaluation of Visual Explanations

Ahmed Osman\*, Leila Arras\*, and Wojciech Samek

Machine Learning Group, Fraunhofer Heinrich Hertz Institute, Germany  
{ahmed.osman,leila.arras,wojciech.samek}@hhi.fraunhofer.de

**Abstract.** Several methods have been proposed to explain the decisions of neural networks in the visual domain via saliency heatmaps (aka relevances/feature importance scores). Thus far, these methods were mainly validated on real-world images, using either pixel perturbation experiments or bounding box localization accuracies. In the present work, we propose instead to evaluate explanations in a restricted and controlled setup using a synthetic dataset of rendered 3D shapes. To this end, we generate a CLEVR-alike visual question answering benchmark with around 40,000 questions, where the ground truth pixel coordinates of relevant objects are known, which allows us to validate explanations in a fair and transparent way. We further introduce two straightforward metrics to evaluate explanations in this setup, and compare their outcomes to standard pixel perturbation using a Relation Network model and three decomposition-based explanation methods: Gradient  $\times$  Input, Integrated Gradients and Layer-wise Relevance Propagation. Among the tested methods, Layer-wise Relevance Propagation was shown to perform best, followed by Integrated Gradients. More generally, we expect the release of our dataset and code to support the development and comparison of methods on a well-defined common ground.

**Keywords:** Interpretability · Evaluation · Ground Truth · Convolutional Neural Network · Relation Network

## 1 Introduction

With the renaissance of neural networks in the last decade, the domain of application of neural network models has been continuously increasing. Indeed these models were shown to reach very good performance on various large-scale prediction tasks, e.g. on the ImageNet recognition Challenge.

At the same time, concerns were raised to whether such high performance is based on genuinely solving a given problem, or if it may in part rely on spurious correlations in the data [12,3,10]. Besides, from an end-user perspective, it might also be highly desirable or even required [5,8] to accompany a model's decision with an *explanation*, to uncover the decision process and trace it back to decisive parts of the input.

---

\* Equal contribution (authors listed in random order)

In the vision domain, the *explanation* can take the form of a heatmap, where each pixel in an input image gets assigned a *relevance* score, indicating its relative contribution to the final decision.

Methods that provide such heatmaps in a direct and unambiguous way include, amongst others, Class Saliency Map [21], Occlusion [24], Gradient  $\times$  Input, Integrated Gradients [23], Layer-wise Relevance Propagation [6], Excitation Backpropagation [26], Guided Backpropagation [22]. Other methods leverage information from additional training data samples or require solving an ad-hoc optimization problem to provide a single heatmap [18,11].

In previous works, these heatmaps were mainly validated on real-world images, either through perturbing pixels accordingly to their relevance and tracking the impact on the model’s prediction, or by using the pixel relevances as an object detection signal. While these evaluations might be justified in a scenario where no ground truth relevant pixels are available for a given task, they could potentially also create a mismatch between the explanation’s primary goal (explain the *current* decision) and the evaluation criterion (track the *change* in model prediction, or identify an object’s *bounding box*).

In the present work, we propose to evaluate explanations *directly* against ground truth pixel coordinates using a restricted setup of synthetic (albeit realistically shaded) images of rendered 3D shapes. To this end, we leverage the CLEVR visual question answering (VQA) data generator, which was initially developed to diagnose VQA models, and augment it with ground truth pixel-level object coordinates to make it suited for evaluating explanations.

We further introduce two novel metrics to quantitatively evaluate explanations in this setup, and apply these metrics onto a Relation Network based model, and on three different explanation methods. We additionally perform a standard perturbation experiment, to check whether the latter analysis leads to consistent results w.r.t. our ground truth approach.

More generally, we expect the release of our code and dataset<sup>1</sup> will encourage the evaluation of explanation methods on a well-defined common basis.

## 2 Related work

A standard approach to evaluate explanations in the visual domain was initially proposed as pixel-flipping or region-perturbation experiment [6,19], and has been widely adopted in previous works [11,7,16,2]. It consists in repeatedly altering a sequence of pixels (or pixel boxes) in an input image, accordingly to their relevance ranking, and measuring the effect of this perturbation on the model’s prediction. The higher the effect, measured e.g. in terms of prediction performance drop, the more accurate was the relevance. One potential issue with this kind of approach is that the model might receive input images that lie outside of the actual training data’s distribution, which could lead to artifacts and unreliable model predictions.

<sup>1</sup> Our dataset and code are available at <https://github.com/ahmedmagdiosman/simply-clevr-dataset>

In contrast, our evaluation approach is based on unmodified input images, from the same distribution as during training.

Another perturbation-based evaluation consists in performing randomizations tests on the model weights and input data, to verify that the explanation indeed depends on both these parameters [1]. While this type of analysis can serve as a first sanity check for explanations, it can not provide a direct quantitative assessment of the explanation’s quality.

A further commonly used approach for evaluating explanations in the visual domain, is to use the pixel relevances for object localization, e.g. by applying a threshold on the relevances, and then computing the Intersection over Union (IoU) or related metrics w.r.t. object bounding box annotations as a measure of relevance accuracy [21,26,25]. This type of evaluation could also be misleading, since it assumes the model’s classification decision is based solely on the object itself, and not on its context or background, which on real-world datasets can not be ensured. Moreover, the IoU metric favors a relevance distribution that closely match the object’s bounding box surface, while a trained classifier might as well rely on parts of this area.

In our synthetic setup, we can ensure that the image’s background is not informative for the model’s prediction, since it is made of the same gray color for all images. Moreover, we can determine the exact position of relevant pixels since we know the true object boundaries. Thus our annotations are unbiased and fine-grained.

Closely related to our work is the evaluation approach taken by [17] who use a synthetic dataset of flowers with known discriminative features (mainly the petal or stem color), and calculate the IoU of visual explanations w.r.t. ground truth masks of the corresponding flower components. In their considered task all flowers have the same size, and each image contains a single flower to classify.

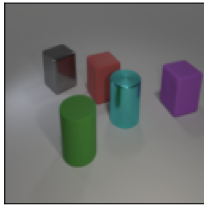
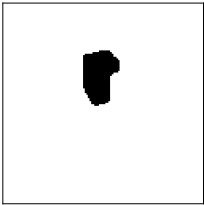
Our VQA setup instead has more variability, each image contains *several* objects with various attributes (3 shapes, 8 colors, 2 sizes and 2 materials), and for each image we generate 4 questions with a different ground truth object as target. This allows us to evaluate the *selectivity* of explanations in a more entangled and realistic setup, where the explanation has to select the right object among multiple objects present in the image.

Lastly, other works relied on the human-centered inspection and validation of visual explanations [23,22,11,18]. While these studies give complementary insights about the usability of explanations from a non-expert end-user perspective, and contribute to an intuitive understanding of the explanation methods, they can not replace an objective and systematic automatic evaluation.

### 3 A Benchmark for Visual Explanations

#### 3.1 Dataset

**Data Generator.** Our benchmark dataset for evaluating explanations was built upon the CLEVR dataset generator [9]. CLEVR is a synthetic VQA task designed to diagnose the reasoning abilities of VQA models by avoiding the biases

Question, Answer	Image	One Object Mask	All Objects Mask
<p><b>The large red object is what shape?</b></p> <p><i>cube</i></p>			
Functional Program:	<i>filter_size → filter_color → unique → query_shape</i>		

**Fig. 1.** A sample data point from our *simply*-CLEVR dataset. The functional program is used to determine which object in the scene is considered as the single ground truth object. We also build a ground truth mask where all objects in the scene are selected.

present in real-world human-annotated VQA datasets [4], and allowing full control on the data generation pipeline. The CLEVR dataset is comprised of a 3-way split of training/validation/test sets with 70,000/15,000/15,000 images and 699,989/149,991/149,988 questions, resp., and the prediction problem is framed as a classification task with 28 possible answers.

CLEVR images contain 3D objects rendered under various lighting directions and positioned on a plane surface, each object having 4 types of attributes (color, material, size, and shape). The image generation encompasses the creation of a *scene graph* which contains all necessary information to describe the scene such as object locations, attributes, and inter-object relations. Further, the question generation is done via a *functional program* and various program templates. The functional program is made of a sequence of basic functions such as querying and comparing attributes, counting objects, and checking the existence of a certain object. Once the functional program is built, it can be applied on a scene graph to yield a ground truth answer. Further, it can be used to identify relevant objects along the question processing pipeline.

In the present work, we will first train a model on the original CLEVR training set, and subsequently, we will evaluate explanations in a restricted CLEVR-like setup, where we generate questions along with ground truth object masks (as those masks are not available in the original CLEVR dataset).

We denote our benchmark dataset as *simply*-CLEVR: it contains simple queries about object attributes, and no inter-object relations, such that we can uniquely identify the *single* relevant object for each question, and use it as a ground truth mask for explanations.

**Image Generation.** To generate the *simply*-CLEVR images, we use the same pipeline as in the CLEVR generator [9]. Additionally, we use the scene graph to create a segmentation mask for each object in the scene (we achieved this in practice by rendering a secondary image where light sources are deactivated and each object gets assigned a unique color). These segmentation masks will be

later used to generate the questions’ ground truth masks. Overall, we generated 10,000 images with each image containing 3 to 10 objects.

**Question Generation.** Second, we generated *simply*-CLEVR questions in the same fashion as in the CLEVR generator [9], except that in order to remove ambiguity in the ground truth masks, we only use a subset of question families where the answer can be inferred by examining only a single object. For instance, for the question “What material is the tiny cyan sphere?”, the relevant object of the question must be the only tiny cyan sphere in the scene. To this end, we only use the question families *query\_shape*, *query\_color*, *query\_size*, *query\_material*, each with 4 simple question templates. For each image, we sample one template from each question family, i.e. we create 4 questions per image. Ill-posed questions are finally discarded (as was done in [9]). This leaves us with a total of 39,761 questions.<sup>2</sup>

**Ground Truth Masks.** Using the object segmentation masks previously generated and each question’s functional program, we can automatically identify the target object for each question. With this information, we generated two types of ground truth masks for evaluating explanations.

*One Object Mask.* The first type of mask generated is based solely on the target object’s pixels, which are marked as True, while remaining objects’ pixels, as well as the background, are set to False.

*All Objects Mask.* The second ground truth mask we generated is less discriminative, and encompasses all objects’ pixels in the scene, those pixels are set to True, while only the scene’s background is set to False. This latter mask will allow us to perform a weak sanity check on the explanation, and verify whether the relevance is indeed assigned to objects and not to the background, since in our synthetic task, by construction, the background shall be uninformative. A sample data point from our *simply*-CLEVR dataset is depicted in Fig. 1.

### 3.2 Evaluation metrics

For visual explanations, evaluation w.r.t. ground truth masks requires heatmaps to be a 2D image with a single channel. Indeed, we care about the spatial location of the relevant objects rather than their channel (color) attributes. For most relevance methods, the original heatmaps mirror the shape of the model input (i.e. 3 channels for RGB images). Thus, there are a number of ways to *pool* the multiple channels down to a single-channel heatmap. Since there is no consensus in the literature on how to perform this pooling step, we evaluate each explanation method using six different pooling techniques.

After obtaining the pooled heatmaps, we utilize two simple metrics for evaluation: a relevance mass accuracy and a relevance rank accuracy. Additionally, we compare our metrics with the traditional pixel perturbation test.

<sup>2</sup> For comparison, the ImageNet test set size is 50,000.

**Pooling techniques.** The six pooling techniques that we utilize in this paper are the following:

$$\begin{aligned}
\text{max-norm: } R_{pool} &= \max(|R_1|, |R_2|, \dots, |R_C|) \\
\text{l2-norm sq: } R_{pool} &= \sum_{i=1}^C R_i^2 \\
\text{l2-norm: } R_{pool} &= \sqrt{\sum_{i=1}^C R_i^2} \\
\text{l1-norm: } R_{pool} &= \sum_{i=1}^C |R_i| \\
\text{sum,abs: } R_{pool} &= \left| \sum_{i=1}^C R_i \right| \\
\text{sum,pos: } R_{pool} &= \max\left(0, \sum_{i=1}^C R_i\right)
\end{aligned} \tag{1}$$

where  $R_{pool}$  is the pooled relevance at the current pixel,  $i$  is the channel index which starts from 1 to the number of channels  $C$  ( $C = 3$  for RGB images) and  $R_i$  is the relevance value at channel  $i$ .

**Relevance Mass Accuracy.** The relevance mass accuracy is computed as the ratio of the sum of relevance values that lie within the ground truth mask over the sum of all relevance values over the entire image. In other words, it measures how much ‘‘mass’’ does the explanation method give to pixels within the ground truth.

It can be written as:

$$\text{Mass Accuracy} = \frac{R_{within}}{R_{total}} \tag{2}$$

$$R_{within} = \sum_{\substack{k=1 \\ \text{s.t. } p_k \in GT}}^K R_{p_k} \tag{3}$$

$$R_{total} = \sum_{k=1}^N R_{p_k} \tag{4}$$

where  $GT$  is the set of pixel locations that lie within the ground truth mask,  $K$  is the number of pixels  $p_k$  in this mask,  $N$  is the total number of pixels in the image, and  $R_{p_k}$  is the relevance value at pixel  $p_k$ .

**Relevance Rank Accuracy.** The relevance rank accuracy measures how much of the high intensity relevances lie within the ground truth. It is calculated by the following steps. Let  $K$  be the size of the ground truth mask. Get the  $K$  highest relevance values. Then count how many of these values lie within the ground truth pixel locations, and divide by the size of the ground truth. Informally, this can be written as:

$$P_{top\ K} = \{p_1, p_2, \dots, p_K \mid R_{p_1} > R_{p_2} > \dots > R_{p_K}\} \quad (5)$$

where  $P_{top\ K}$  is the set of pixels with relevance values  $R_{p_1}, R_{p_2}, \dots, R_{p_K}$  sorted in decreasing order until the  $K$ -th pixel. Then, the rank accuracy is computed as:

$$\text{Rank Accuracy} = \frac{|P_{top\ K} \cap GT|}{|GT|} \quad (6)$$

### 3.3 Pixel perturbation analysis

The pixel perturbation analysis replaces the highest intensity relevance values with an uninformative pixel value and gauges the model’s response induced by this change. In this work, we calculate a mean value per channel over the whole CLEVR training set to be used as our uninformative pixel value. After pooling, we gradually replace the highest-valued relevance pixels one-by-one with the uninformative pixel, up to the 200-th most relevant pixel. After each pixel perturbation step, we measure the drop in model prediction accuracy (for this experiment we start by considering all correctly predicted data points, therefore the start accuracy is 1.0). According to this evaluation method, the accuracy drop induced by pixel perturbation is inversely proportional to the accuracy of the explanation.

## 4 Experiments

### 4.1 Model

The model we consider for evaluation is a Relation Network (RN) model [20], a simple architecture with near perfect prediction accuracy on the CLEVR dataset (the authors report 95.5% accuracy on the CLEVR test set). We chose this model because, among the architectures that perform well on the CLEVR dataset, it is arguably the simplest one, and we didn’t want to obfuscate our evaluation of explanation methods by the complexity of the neural network model. The RN model is made of very common neural network layers: standard convolutional and batchnorm layers, fully-connected layers, element-wise summation and ReLU activations, plus an LSTM for processing the question.

More precisely, a 4-layer CNN is used to extract feature maps from the image. Then, the pixels in the last convolutional feature maps are pair-wise concatenated with the question representation obtained from the last hidden state of

the LSTM. These representations are passed through a 4-layer MLP of fully-connected layers, summed-up in place, and finally fed to a 3-layer MLP of fully-connected layers for classification.

Since the original authors [20] did not release their code, we re-implement their model and train it from scratch on the CLEVR training set, using the validation set for hyperparameter tuning. As an image preprocessing step, we rescaled the images to the range  $[0, 1]$  (we did not center the data since the RN model contains batchnorm layers), and during training dropout was applied to the second to last layer (for more details on the implementation and training we refer to the Appendix).

Our trained model reaches 93.3% accuracy on the CLEVR test set, and 98.2% accuracy on our *simply*-CLEVR dataset. Hence, it solves the latter task almost perfectly and can be used for evaluating the quality of explanations.

## 4.2 Explanation methods

As a first step towards ground truth evaluation of visual explanations, in this work we consider three different general purpose explanation methods, which do not require any additional training or sampling, and can be computed in a straightforward and deterministic manner (independently of the choice of the sampling procedure or hyperparameter initialization), and leave the exploration of additional methods for future work.

To start, let us define some notations. We suppose given  $f_c(\cdot)$  a real-valued prediction function for some *target* class  $c$  (typically the classifier’s *predicted* class is used), and an input image  $\mathbf{x} \in \mathbb{R}^{C \times H \times W}$  (or  $\mathbb{R}_{\geq 0}^{C \times H \times W}$ , depending on the preprocessing), where  $C$  is the number of input channels,  $H$  is the image height and  $W$  is the image width.

An explanation method then provides for each single input dimension  $x_i$ <sup>3</sup> a scalar *relevance* value  $R_{x_i} \in \mathbb{R}$  (or  $\mathbb{R}_{\geq 0}$ , depending on the explanation method).

These relevances can finally be pooled along the channel axis (as was described in Section 3.2) to obtain a positive-valued relevance heatmap of size  $H \times W$ , which can be displayed in 2D and superimposed to the original image for manual inspection, or serve as a basis for quantitative evaluation.

Note that since our model is a VQA classifier, a relevance value can also be obtained for each word embedding dimension of the input question, and that the prediction function  $f_c(\cdot)$  takes both the image  $\mathbf{x}$  and the question  $\mathbf{q}$  as inputs. However, for simplifying notations, we omit the dependence on the question, since our subject in this work is to evaluate the explanations on the image-side.

**Gradient  $\times$  Input.** One method to obtain the single relevances  $R_{x_i}$ , which was often used as a baseline in previous works, is based on the partial derivative of

<sup>3</sup> For brevity, we index all input variables by  $i$ , note though that  $i$  corresponds to a specific pixel location in horizontal and vertical direction and to a specific channel.

the classifier’s prediction function w.r.t. the input image, element-wise multiplied with the image’s variables, we denote it as Gradient  $\times$  Input (GI):

$$R_{x_i} = \frac{\partial f_c}{\partial x_i}(\mathbf{x}) \cdot x_i \quad (7)$$

The partial derivatives can be obtained in one gradient backward pass.

**Integrated Gradients.** Another method which was introduced by [23] is Integrated Gradients (IG). The relevances  $R_{x_i}$  are based on approximating the following integral:

$$R_{x_i} = (x_i - x'_i) \cdot \int_{\alpha=0}^1 \frac{\partial f_c(\mathbf{x}' + \alpha \cdot (\mathbf{x} - \mathbf{x}'))}{\partial x_i} d\alpha, \quad (8)$$

where  $\mathbf{x}'$  is a *baseline* image to be chosen by the end-user. It should ideally be an image with near-zero prediction score and containing no signal. The original authors used a zero-valued image, i.e. a black image, for that purpose.

In our experiments we also used a zero-valued baseline. Additionally we experimented with two other baselines: namely, the mean image as well as the mean channel values over the flattened input images, which we computed over the CLEVR training data. Since the CLEVR images contain a grey background, this resulted in two grey-valued baselines. We found the mean channel baseline to perform best, followed by the mean image results, and both performing better than the zero baseline. Therefore we only report results with the mean channel baseline (see Appendix for additional results).

Another choice to be made when employing the Integrated Gradients method is the number of integration steps used for integral approximation. To this end, one can exploit the completeness property of Integrated Gradients:

$$\sum_i R_{x_i} = f_c(\mathbf{x}) - f_c(\mathbf{x}') \quad (9)$$

In our experiments we ensure that the relative error is lower than 0.01,<sup>4</sup> and discard from our results data points with higher errors (the original authors suggest an error bound of 0.05).

**Layer-wise Relevance Propagation.** An additional method we consider is Layer-wise Relevance Propagation (LRP). It was initially proposed in [6] and later justified via Deep Taylor Decomposition [14,15]. It consists in redistributing the model’s prediction  $f_c(\mathbf{x})$  via a custom backward pass that follows a local conservation principle. During this backward pass each neuron in the network gets assigned its own relevance value, up to the input layer neurons.

In practice, on ReLU element-wise activation layers, the relevance is backward propagated as the identity, while weighted linear connections serve to

<sup>4</sup> We tried the following number of integration steps: [300, 1000, 3000, 10000, 30000], and used the Riemann sum with midpoint rule for integral approximation.

switch the relevance in *proportion* to neuron contributions in the forward pass. Given a linear layer with the forward pass equation  $z_j = \sum_i z_i w_{ij} + b_j$ , two main LRP backward propagation rules can be used to compute the neuron relevances  $R_i$ , given the relevances of the connected higher-layer neurons  $R_j$ . One is the  $\epsilon$ -rule:

$$R_i = \sum_j \frac{z_i \cdot w_{ij}}{z_j + \epsilon \cdot \text{sign}(z_j)} \cdot R_j, \quad (10)$$

where  $\epsilon$  is a stabilizer (we use  $\epsilon = 0.001$ ), the other is the  $\alpha_1, \beta_0$ -rule:

$$R_i = \sum_j \frac{(z_i \cdot w_{ij})^+}{\sum_i (z_i \cdot w_{ij})^+ + (b_j)^+} \cdot R_j, \quad (11)$$

where  $(\cdot)^+$  denotes the  $\max(0, \cdot)$  operation. Note that when using the latter propagation rule LRP is equivalent to Excitation Backpropagation [26].

We experimented with either using each rule uniformly along the whole network, or a combination of both rules where we employ the  $\epsilon$ -rule for fully-connected layers and the  $\alpha_1, \beta_0$ -rule for convolutional and batchnorm layers. Using the  $\alpha_1, \beta_0$ -rule for all layers led to the best results, therefore we report only this variant in our results.

Note that there exist other LRP rules that were proposed in the literature, in particular for input layers [14], and that the authors of [13] further recommend to subsume consecutive convolutional and batchnorm layers into a single linear layer before applying LRP. However, we leave the exploration of further LRP variants for future work.

## 5 Results and Discussion

Given the trained model, we evaluate the explanation methods on the *simply-CLEVR* dataset consisting of 39,761 data points. We compute both the relevance mass accuracy, as well as the relevance rank accuracy, using either a single object or all objects as ground truth. Our results are compiled in Tables 1 to 4. Fig. 2 illustrates the visual explanations on a sample data point.

In particular, we consider two subsets of data points: first all correctly predicted points, second the correctly points which were predicted with very high confidence (softmax probability  $> 0.9999$ ). The latter subset enables us to verify whether the relevance accuracy increases with the classifier’s confidence, since intuitively, a model shall focus more on the correct object when it is sure of it’s prediction, and conversely when the classifier is more confused, e.g. when the target ground truth object is small or partly occluded, then the relevance might be less focused on the correct object and be more diffused.

Indeed, we observe the latter phenomenon when using a single object as ground truth (Tables 1 and 3), both for LRP and IG, while for LRP this effect is more pronounced (the standard deviation also decreases). We observed a similar increase in relevance accuracy when considering a subset of data points for which the ground truth single object mask’s size (in terms of number of pixels) was superior to the mean mask size over the dataset (see Appendix). With GI we

**Table 1.** Relevance accuracy using the *mass metric* and a *single object* as ground truth (this is the object identified by the data point’s question), for different types of relevance pooling along the image’s channels (the maximum accuracy per explanation method is highlighted bold). We consider different data subsets (the corresponding number of data points is indicated in parenthesis)

Mass Metric Single Object GT	GI		IG		LRP	
	mean (std)	median	mean (std)	median	mean (std)	median
- all correctly predicted (39027 points)						
max-norm	0.15 (0.12)	0.11	0.39 (0.21)	0.37	0.56 (0.20)	0.60
l2-norm sq	<b>0.29 (0.24)</b>	<b>0.22</b>	<b>0.68 (0.28)</b>	<b>0.78</b>	<b>0.80 (0.20)</b>	<b>0.87</b>
l2-norm	0.15 (0.12)	0.11	0.39 (0.21)	0.37	0.55 (0.19)	0.57
l1-norm	0.15 (0.12)	0.11	0.38 (0.21)	0.36	0.53 (0.18)	0.56
sum,abs	0.15 (0.13)	0.11	0.38 (0.21)	0.35	0.53 (0.18)	0.56
sum,pos	0.15 (0.13)	0.11	0.40 (0.21)	0.39	0.53 (0.18)	0.56
- correctly predicted with softmax probability > 0.9999 (29324 points)						
max-norm	0.15 (0.12)	0.11	0.41 (0.20)	0.40	0.61 (0.18)	0.64
l2-norm sq	<b>0.29 (0.23)</b>	<b>0.23</b>	<b>0.71 (0.27)</b>	<b>0.81</b>	<b>0.84 (0.15)</b>	<b>0.89</b>
l2-norm	0.15 (0.12)	0.11	0.41 (0.20)	0.39	0.59 (0.16)	0.61
l1-norm	0.15 (0.12)	0.11	0.40 (0.20)	0.39	0.57 (0.15)	0.59
sum,abs	0.15 (0.13)	0.11	0.40 (0.21)	0.38	0.57 (0.15)	0.59
sum,pos	0.15 (0.13)	0.11	0.43 (0.21)	0.41	0.57 (0.15)	0.59

**Table 2.** Relevance accuracy using the *mass metric* and *all objects* as ground truth (these are all objects present in the image), for different types of relevance pooling along the image’s channels (the maximum accuracy per explanation method is highlighted bold). We consider different data subsets (the corresponding number of data points is indicated in parenthesis)

Mass Metric All Objects GT	GI		IG		LRP	
	mean (std)	median	mean (std)	median	mean (std)	median
- all correctly predicted (39027 points)						
max-norm	0.31 (0.12)	0.29	0.78 (0.10)	0.80	0.84 (0.07)	0.85
l2-norm sq	<b>0.43 (0.21)</b>	<b>0.39</b>	<b>0.97 (0.04)</b>	<b>0.98</b>	<b>0.90 (0.10)</b>	<b>0.94</b>
l2-norm	0.30 (0.12)	0.29	0.77 (0.10)	0.78	0.81 (0.08)	0.82
l1-norm	0.30 (0.12)	0.28	0.76 (0.11)	0.77	0.78 (0.08)	0.79
sum,abs	0.30 (0.12)	0.29	0.76 (0.11)	0.78	0.78 (0.08)	0.79
sum,pos	0.30 (0.12)	0.29	0.77 (0.10)	0.78	0.78 (0.08)	0.79
- correctly predicted with softmax probability > 0.9999 (29324 points)						
max-norm	0.29 (0.12)	0.28	0.77 (0.10)	0.79	0.84 (0.07)	0.86
l2-norm sq	<b>0.42 (0.21)</b>	<b>0.38</b>	<b>0.97 (0.03)</b>	<b>0.98</b>	<b>0.90 (0.10)</b>	<b>0.94</b>
l2-norm	0.29 (0.12)	0.27	0.76 (0.11)	0.78	0.81 (0.08)	0.82
l1-norm	0.28 (0.12)	0.27	0.75 (0.11)	0.77	0.78 (0.08)	0.79
sum,abs	0.29 (0.12)	0.27	0.75 (0.11)	0.77	0.78 (0.08)	0.79
sum,pos	0.29 (0.12)	0.27	0.76 (0.11)	0.78	0.78 (0.08)	0.79

**Table 3.** Relevance accuracy using the *rank metric* and a *single object* as ground truth (this is the object identified by the data point’s question), for different types of relevance pooling along the image’s channels (the maximum accuracy per explanation method is highlighted bold). We consider different data subsets (the corresponding number of data points is indicated in parenthesis)

Rank Metric Single Object GT	GI		IG		LRP	
	mean (std)	median	mean (std)	median	mean (std)	median
- all correctly predicted (39027 points)						
max-norm	<b>0.28 (0.17)</b>	<b>0.27</b>	<b>0.53 (0.18)</b>	<b>0.55</b>	<b>0.69 (0.18)</b>	<b>0.74</b>
l2-norm sq	0.27 (0.17)	0.25	0.52 (0.18)	0.55	0.68 (0.16)	0.73
l2-norm	0.27 (0.17)	0.25	0.52 (0.18)	0.55	0.68 (0.16)	0.73
l1-norm	0.26 (0.16)	0.24	0.51 (0.18)	0.54	0.67 (0.15)	0.71
sum.abs	0.24 (0.16)	0.23	0.47 (0.18)	0.50	0.67 (0.15)	0.71
sum.pos	0.18 (0.10)	0.18	0.34 (0.10)	0.36	0.67 (0.15)	0.71
- correctly predicted with softmax probability > 0.9999 (29324 points)						
max-norm	<b>0.28 (0.17)</b>	<b>0.27</b>	<b>0.55 (0.17)</b>	<b>0.58</b>	<b>0.73 (0.14)</b>	<b>0.77</b>
l2-norm sq	0.27 (0.17)	0.26	0.55 (0.17)	0.57	0.72 (0.13)	0.75
l2-norm	0.27 (0.17)	0.26	0.55 (0.17)	0.57	0.72 (0.13)	0.75
l1-norm	0.26 (0.16)	0.24	0.54 (0.17)	0.56	0.71 (0.11)	0.73
sum.abs	0.24 (0.16)	0.23	0.50 (0.17)	0.52	0.71 (0.11)	0.73
sum.pos	0.19 (0.10)	0.18	0.35 (0.09)	0.37	0.71 (0.11)	0.73

**Table 4.** Relevance accuracy using the *rank metric* and *all objects* as ground truth (these are all objects present in the image), for different types of relevance pooling along the image’s channels (the maximum accuracy per explanation method is highlighted bold). We consider different data subsets (the corresponding number of data points is indicated in parenthesis)

Rank Metric All Objects GT	GI		IG		LRP	
	mean (std)	median	mean (std)	median	mean (std)	median
- all correctly predicted (39027 points)						
max-norm	<b>0.31 (0.09)</b>	<b>0.30</b>	<b>0.72 (0.07)</b>	<b>0.72</b>	<b>0.76 (0.08)</b>	<b>0.77</b>
l2-norm sq	0.30 (0.09)	0.30	0.71 (0.07)	0.71	0.73 (0.08)	0.74
l2-norm	0.30 (0.09)	0.30	0.71 (0.07)	0.71	0.73 (0.08)	0.74
l1-norm	0.29 (0.09)	0.29	0.69 (0.08)	0.70	0.70 (0.08)	0.72
sum.abs	0.28 (0.08)	0.28	0.65 (0.08)	0.66	0.70 (0.08)	0.72
sum.pos	0.23 (0.06)	0.23	0.40 (0.04)	0.40	0.70 (0.08)	0.72
- correctly predicted with softmax probability > 0.9999 (29324 points)						
max-norm	<b>0.30 (0.09)</b>	<b>0.30</b>	<b>0.71 (0.07)</b>	<b>0.72</b>	<b>0.75 (0.08)</b>	<b>0.77</b>
l2-norm sq	0.29 (0.09)	0.29	0.70 (0.08)	0.71	0.73 (0.08)	0.74
l2-norm	0.29 (0.09)	0.29	0.70 (0.08)	0.71	0.73 (0.08)	0.74
l1-norm	0.29 (0.09)	0.28	0.69 (0.08)	0.69	0.70 (0.08)	0.71
sum.abs	0.28 (0.08)	0.27	0.65 (0.08)	0.66	0.70 (0.08)	0.71
sum.pos	0.23 (0.06)	0.23	0.40 (0.04)	0.40	0.70 (0.08)	0.71

did not observe this phenomenon, and generally, GI performed very poorly in all experiments.

In terms of comparing LRP to IG, LRP performed best in 3 out of 4 test cases, while IG performed best in terms of relevance mass accuracy when considering all objects as ground truth (Table 2).

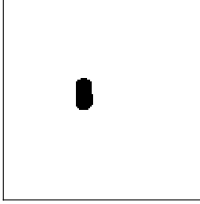
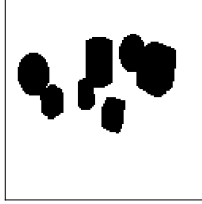
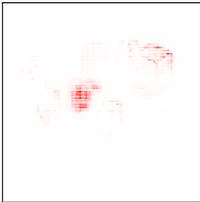
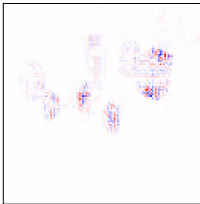
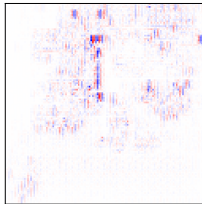
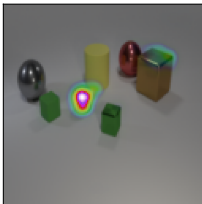
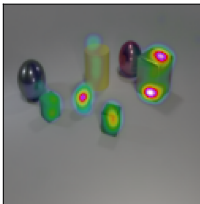
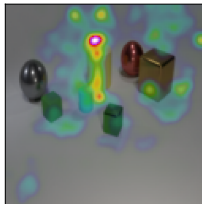
The mass accuracy is in general very sensitive to the relevance pooling type and to extremal relevance values, and for this metric the l2-norm squared performed best for all explanations. The rank accuracy is less sensitive to the type of pooling, here the max-norm pooling gave the best results for all methods.

Overall, on single object ground truths, the best performing method, LRP, reached 0.80 mean mass accuracy, and 0.69 mean rank accuracy (Table 1 and 3, first row). This leaves room for improvements for future work, and shows that our benchmark evaluation can be used by follow-up works for improving and developing explanations.

However, we would like to point out that it remains an open question to whether the 1.0 relevance accuracy upper bound can be reached by an explanation method, since part of the low relevance accuracy results might come from the classifier which is uncertain or confused on some data points. Still, this does not invalidate our evaluation approach since the classifier’s uncertainty is the same for all explanation methods. Further, our dataset contains some difficult to classify data points, where the ground truth object is small and partly occluded (the ground truth mask for single objects varies between 40 and 2040 pixels, with mean size of 428 pixels).

On the perturbation experiment (see Fig. 3), we get consistent results with our ground truth evaluation: GI performs poorly, and LRP performs slightly better than IG. One key difference between both explanations methods is that LRP’s relevance can be computed in one backward pass through the network, while IG requires multiple gradient backward passes. Moreover, in our setup it is relatively clear how to choose the baseline image for IG, since we know which pixel value is uninformative for the trained model. On a real-world dataset it might be less clear how to define a good IG baseline.

Finally, we would like to point out a limitation of our approach: our ground truth masks do not take into the object’s shadows, while in principle the model can use them for answering certain questions (such as queries on the object’s shape). However, we preferred using a dataset with real-world looking illumination conditions and shadows, rather than using a more artificial task (such as the sort-of-CLEVR task from [20]) for evaluating explanations.

Question, Answer	Image	One Object Mask	All Objects Mask
<p>The cyan rubber thing is what size?</p> <p><i>small</i></p>			
Method	LRP	IG	GI
raw heatmap			
overlayed heatmap			

**Fig. 2.** Heatmaps for different explanation methods, on a sample data point from the *simply*-CLEVR dataset. For the raw heatmap visualization the relevances are simply summed up along the channels and color-coded (red for positive, blue for negative)

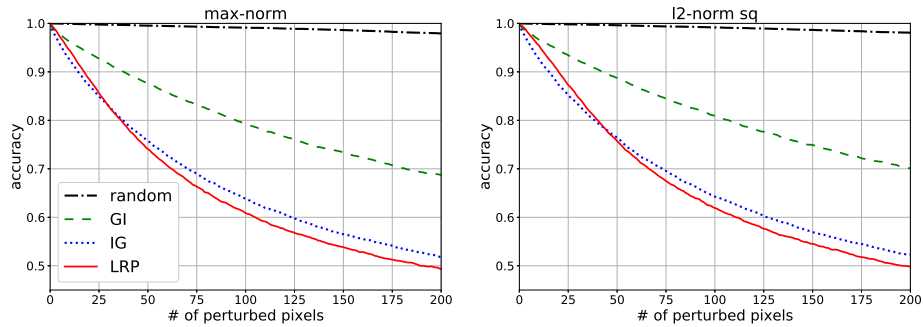


**Fig. 3.** Decrease in model accuracy as a function of the number of perturbed pixels. Pixels are perturbed one-by-one and replaced by the mean channel value, in decreasing order of their relevance. All correctly classified data points are considered for this experiment, as well as two types of relevance pooling (indicated on top)

## 6 Conclusion

In this paper, we proposed a synthetic VQA dataset with explanation ground truth masks, and two simple relevance accuracy metrics for evaluating explanations. While our evaluation approach is simple, it enables an unbiased and transparent comparison of explanation methods, and it uses data from the same distribution as during model training. We release our dataset and code for encouraging further work in this direction.

## 7 Acknowledgments

This work was partly supported by the German Ministry for Education and Research as BIFOLD - Berlin Institute for the Foundations of Learning and Data (ref. 01IS18025A and ref 01IS18037A).

## References

1. Adebayo, J., Gilmer, J., Muelly, M., Goodfellow, I., Hardt, M., Kim, B.: Sanity Checks for Saliency Maps. In: *Advances in Neural Information Processing Systems* 31 (NIPS), pp. 9505–9515 (2018)
2. Ancona, M., Ceolini, E., Öztireli, C., Gross, M.: Towards better understanding of gradient-based attribution methods for deep neural networks. In: *International Conference on Learning Representations (ICLR)* (2018)
3. Anne Hendricks, L., Burns, K., Saenko, K., Darrell, T., Rohrbach, A.: Women also Snowboard: Overcoming Bias in Captioning Models. In: *Proceedings of the European Conference on Computer Vision (ECCV)*. pp. 793–811 (2018)
4. Antol, S., Agrawal, A., Lu, J., Mitchell, M., Batra, D., Zitnick, C.L., Parikh, D.: VQA: Visual Question Answering. In: *International Conference on Computer Vision (ICCV)*. pp. 2425–2433 (2015)
5. Arrieta, A.B., Diaz-Rodriguez, N., Ser, J.D., Bennetot, A., Tabik, S., Barbado, A., Garcia, S., Gil-Lopez, S., Molina, D., Benjamins, R., Chatila, R., Herrera, F.: Explainable Artificial Intelligence (XAI): Concepts, Taxonomies, Opportunities and Challenges toward Responsible AI. *arXiv:1910.10045* (2019)
6. Bach, S., Binder, A., Montavon, G., Klauschen, F., Müller, K.R., Samek, W.: On Pixel-Wise Explanations for Non-Linear Classifier Decisions by Layer-Wise Relevance Propagation. *PLoS ONE* **10**(7), e0130140 (2015)
7. Chen, J., Song, L., Wainwright, M., Jordan, M.: Learning to Explain: An Information-Theoretic Perspective on Model Interpretation. In: *Proceedings of the 35th International Conference on Machine Learning (ICML)*. pp. 883–892 (2018)
8. EU-GDPR: Regulation (EU) 2016/679 of the European Parliament and of the Council of 27 April 2016 on the protection of natural persons with regard to the processing of personal data and on the free movement of such data, and repealing Directive 95/46/EC (General Data Protection Regulation). *Official Journal of the European Union L 119* **59**, 1–88 (2016)
9. Johnson, J., Hariharan, B., v. d. Maaten, L., Fei-Fei, L., Zitnick, C.L., Girshick, R.: CLEVR: A Diagnostic Dataset for Compositional Language and Elementary Visual Reasoning. In: *Proceedings of the Conference on Computer Vision and Pattern Recognition (CVPR)*. pp. 1988–1997 (2017)

10. Lapuschkin, S., Waldchen, S., Binder, A., Montavon, G., Samek, W., Muller, K.R.: Unmasking Clever Hans Predictors and Assessing What Machines Really Learn. *Nature Communications* **10**, 1096 (2019)
11. Lundberg, S.M., Lee, S.I.: A Unified Approach to Interpreting Model Predictions. In: *Advances in Neural Information Processing Systems 30 (NIPS)*. pp. 4765–4774 (2017)
12. Manjunatha, V., Saini, N., Davis, L.S.: Explicit Bias Discovery in Visual Question Answering Models. In: *Proceedings of the Conference on Computer Vision and Pattern Recognition (CVPR)*. pp. 9562–9571 (2019)
13. Montavon, G., Binder, A., Lapuschkin, S., Samek, W., Muller, K.R.: Layer-Wise Relevance Propagation: An Overview. In: *Explainable AI: Interpreting, Explaining and Visualizing Deep Learning*, pp. 193–209. *Lecture Notes in Computer Science*, volume 11700, Springer (2019)
14. Montavon, G., Lapuschkin, S., Binder, A., Samek, W., Muller, K.R.: Explaining nonlinear classification decisions with deep Taylor decomposition. *Pattern Recognition* **65**, 211–222 (2017)
15. Montavon, G., Samek, W., Muller, K.: Methods for Interpreting and Understanding Deep Neural Networks. *Digital Signal Processing* **73**, 1–15 (2018)
16. Morcos, A.S., Barrett, D.G., Rabinowitz, N.C., Botvinick, M.: On the importance of single directions for generalization. In: *International Conference on Learning Representations (ICLR)* (2018)
17. Oramas, J., Wang, K., Tuytelaars, T.: Visual Explanation by Interpretation: Improving Visual Feedback Capabilities of Deep Neural Networks. In: *International Conference on Learning Representations (ICLR)* (2019)
18. Ribeiro, M.T., Singh, S., Guestrin, C.: “Why Should I Trust You?”: Explaining the Predictions of Any Classifier. In: *Proceedings of the 22nd ACM SIGKDD International Conference on Knowledge Discovery and Data Mining*. pp. 1135–1144 (2016)
19. Samek, W., Binder, A., Montavon, G., Lapuschkin, S., Muller, K.R.: Evaluating the Visualization of what a Deep Neural Network has learned. *IEEE Transactions on Neural Networks and Learning Systems* **28**(11), 2660–2673 (2017)
20. Santoro, A., Raposo, D., Barrett, D.G., Malinowski, M., Pascanu, R., Battaglia, P., Lillicrap, T.: A Simple Neural Network Module for Relational Reasoning. In: *Advances in Neural Information Processing Systems 30 (NIPS)*. pp. 4967–4976 (2017)
21. Simonyan, K., Vedaldi, A., Zisserman, A.: Deep Inside Convolutional Networks: Visualising Image Classification Models and Saliency Maps. In: *International Conference on Learning Representations - Workshop track (ICLR)* (2014)
22. Springenberg, J.T., Dosovitskiy, A., Brox, T., Riedmiller, M.: Striving for Simplicity: The All Convolutional Net. In: *International Conference on Learning Representations - Workshop track (ICLR)* (2015)
23. Sundararajan, M., Taly, A., Yan, Q.: Axiomatic Attribution for Deep Networks. In: *Proceedings of the 34th International Conference on Machine Learning (ICML)*. pp. 3319–3328 (2017)
24. Zeiler, M.D., Fergus, R.: Visualizing and Understanding Convolutional Networks. In: *Proceedings of the European Conference on Computer Vision (ECCV)*. pp. 818–833 (2014)
25. Zhang, J., Bargal, S.A., Lin, Z., Brandt, J., Shen, X., Sclaroff, S.: Top-Down Neural Attention by Excitation Backprop. *International Journal of Computer Vision* **126**(10), 1084–1102 (2018)

26. Zhang, J., Lin, Z., Brandt, J., Shen, X., Sclaroff, S.: Top-Down Neural Attention by Excitation Backprop. In: Proceedings of the European Conference on Computer Vision (ECCV). pp. 543–559 (2016)

# Appendix

## A Additional Heatmaps

**Correctly predicted.** In Fig. 4 and 5, we provide visual explanations for correctly predicted data points.

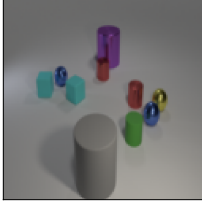
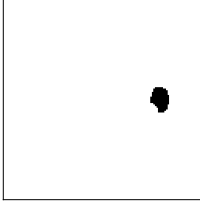
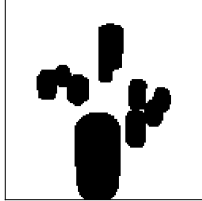
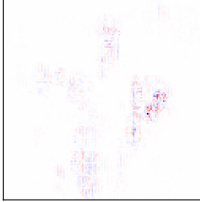
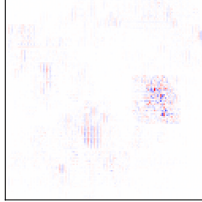
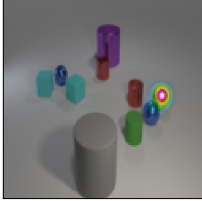
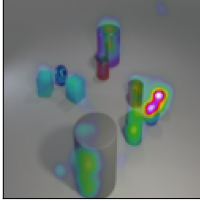
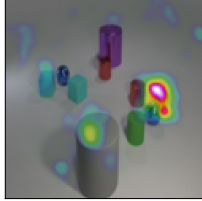
Fig. 4 shows a rich scene with 10 objects, yet all the explanation methods focus on the target object of the question, the small yellow ball, though the LRP heatmap is more concentrated on this object.

Fig. 5 shows a scene where the target object of the question, the small brown ball, is partly occluded. Here, only IG delivers a qualitatively clean explanation, while the other methods produce noisy heatmaps. The LRP heatmap also presents a checkerboard artifact on the bottom of the scene’s background. In practice, we rarely observed such an artifact in the images’ background for the LRP method. Still, this example shows that the LRP variant we used in our experiments might not be optimal (in particular, we expect the combination of convolutional and batchnorm layers into one linear layer before applying LRP, as suggested in [13], might remove such pattern which we would explore in future work).

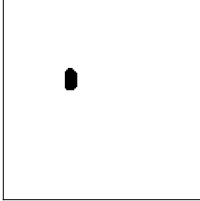
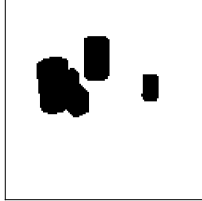
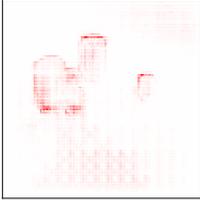
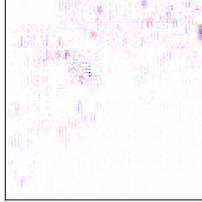
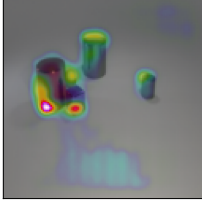
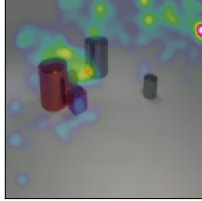
**Falsely predicted.** In Fig. 6 and 7, we provide visual explanations for falsely predicted data points.

In Fig. 6, the question is about the yellow metallic sphere. However, according to the explanations, in particular for the LRP heatmap, the model is instead focusing on the yellow cube, which is consistent with the model’s predicted answer.

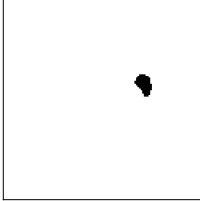
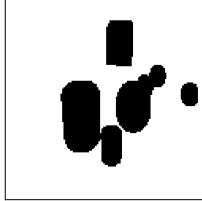
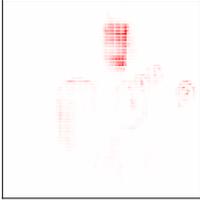
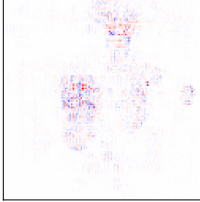
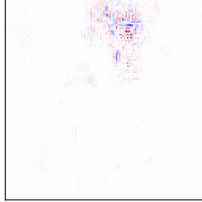
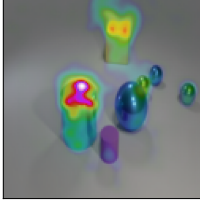
Lastly, Fig. 7 shows a difficult to classify data point: the target object of the question, which is the yellow rubber ball next to the green cylinder is highly occluded. According to the LRP and GI explanations, the model is instead focusing on the matte little cube next to the big red cylinder, and according to the IG explanation it may also have considered the small metallic sphere instead, which again is consistent with the model’s answer.

Question, Answer	Image	One Object Mask	All Objects Mask
<b>What is the small yellow sphere made of?</b> <i>metal</i>			
Method	LRP	IG	GI
raw heatmap			
overlayed heatmap			
Metric			
<b>Single Object GT</b>			
Mass	<b>0.56</b>	0.09	0.09
Rank	<b>0.69</b>	0.26	0.35
<b>All Objects GT</b>			
Mass	<b>0.84</b>	0.68	0.39
Rank	0.60	<b>0.62</b>	0.34

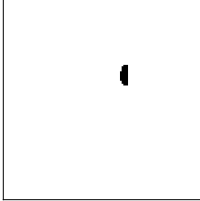
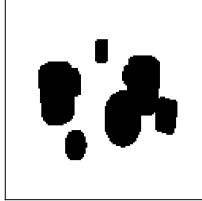
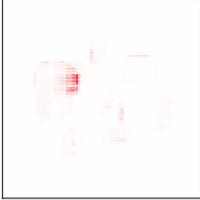
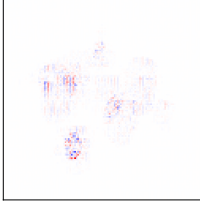
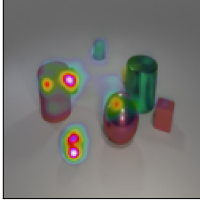
**Fig. 4.** Heatmaps on a *correctly* predicted data point from the *simply-CLEVR* dataset. Evaluation metrics show a quantitative score that can be compared across methods. We use *sum, abs* pooling to compute the relevance accuracy (since it is the most natural pooling method to compare with the raw heatmap visualization).

Question, Answer	Image	One Object Mask	All Objects Mask
<p><b>The brown matte thing has what size?</b> true: <i>small</i></p>			
Method	LRP	IG	GI
raw heatmap			
overlayed heatmap			
Metric			
<b>Single Object GT</b>			
Mass	0.04	<b>0.10</b>	0.02
Rank	0.08	<b>0.19</b>	0.02
<b>All Objects GT</b>			
Mass	0.43	<b>0.66</b>	0.12
Rank	0.49	<b>0.68</b>	0.14

**Fig. 5.** Heatmaps on a *correctly* predicted data point from the *simply-CLEVR* dataset. Evaluation metrics show a quantitative score that can be compared across methods. We use *sum, abs* pooling to compute the relevance accuracy (since it is the most natural pooling method to compare with the raw heatmap visualization).

Question, Answer	Image	One Object Mask	All Objects Mask
<b>What shape is the yellow shiny thing?</b> true: <i>sphere</i> predicted: <i>cube</i>			
Method	LRP	IG	GI
raw heatmap			
overlayed heatmap			
Metric			
<b>Single Object GT</b>			
Mass	<b>0.02</b>	0.02	0.00
Rank	0.00	<b>0.03</b>	0.00
<b>All Objects GT</b>			
Mass	<b>0.80</b>	0.56	0.32
Rank	<b>0.64</b>	0.58	0.23

**Fig. 6.** Heatmaps on a *falsely* predicted data point from the *simply-CLEVR* dataset. Evaluation metrics show a quantitative score that can be compared across methods. We use *sum, abs* pooling to compute the relevance accuracy (since it is the most natural pooling method to compare with the raw heatmap visualization).

Question, Answer	Image	One Object Mask	All Objects Mask
<b>What is the color of the rubber ball?</b> true: <i>yellow</i> predicted: <i>brown</i>			
Method	LRP	IG	GI
raw heatmap			
overlayed heatmap			
Metric			
<b>Single Object GT</b>			
Mass	0.00	0.00	0.00
Rank	0.00	0.00	0.00
<b>All Objects GT</b>			
Mass	0.76	<b>0.79</b>	0.30
Rank	<b>0.72</b>	0.71	0.28

**Fig. 7.** Heatmaps on a *falsely* predicted data point from the *simply-CLEVR* dataset. Evaluation metrics show a quantitative score that can be compared across methods. We use *sum, abs* pooling to compute the relevance accuracy (since it is the most natural pooling method to compare with the raw heatmap visualization).

## B Additional Relevance Accuracy Evaluation

**Ground truth mask size greater than mean.** We explored whether the relevance accuracy increases when the ground truth mask size for single objects is greater than the mean size of all single-object ground truth masks in the *simply-CLEVR* dataset, i.e. 428 pixels.

Our results are reported in Tables 5-6, and are to be contrasted with the results from Table 1 and 3 of the main paper, which contain all correctly predicted data points. With this experiment, we try to exclude difficult to classify data points, such as occluded objects.

Indeed, we observe an improvement between 0.05 and 0.12 in mean mass accuracy, and between 0.03 and 0.08 in mean rank accuracy, for all explanation methods (for LRP the increase is the lowest, but this method still has the highest mean accuracy and lowest standard deviation overall, when considering single objects as ground truth).

This means that when the target object of the question is bigger (in terms of pixels), and thus shall be easier to identify by the model, it is reflected in an increase of the relevance accuracy on the ground truth object. This highlights the fact that the relevance accuracy’s absolute value does not only depend on the quality of an explanation method, but also on the difficulty of the current prediction.

**Table 5.** Relevance accuracy using the *mass metric* and a *single object* as ground truth, for different types of relevance pooling. Here we consider a different data subset: the correctly predicted points with a **ground truth mask > 428 pixels** (cf. Table 1 in the main paper, first row)

Mass Metric Single Object GT	GI		IG		LRP	
	mean (std)	median	mean (std)	median	mean (std)	median
- correctly predicted with ground truth mask > 428 pixels (15935 points)						
max-norm	0.23 (0.13)	0.21	0.54 (0.17)	0.55	0.66 (0.16)	0.69
l2-norm sq	<b>0.41 (0.25)</b>	<b>0.38</b>	<b>0.78 (0.23)</b>	<b>0.88</b>	<b>0.85 (0.15)</b>	<b>0.90</b>
l2-norm	0.23 (0.13)	0.20	0.53 (0.17)	0.54	0.64 (0.15)	0.67
l1-norm	0.23 (0.13)	0.20	0.53 (0.17)	0.53	0.63 (0.13)	0.65
sum,abs	0.23 (0.14)	0.21	0.52 (0.19)	0.53	0.63 (0.13)	0.65
sum,pos	0.23 (0.14)	0.21	0.54 (0.18)	0.55	0.63 (0.13)	0.65

**Table 6.** Relevance accuracy using the *rank metric* and a *single object* as ground truth, for different types of relevance pooling. Here we consider a different data subset: the correctly predicted points with a **ground truth mask > 428 pixels** (cf. Table 3 in the main paper, first row)

Rank Metric Single Object GT	GI		IG		LRP	
	mean (std)	median	mean (std)	median	mean (std)	median
- correctly predicted with ground truth mask > 428 pixels (15935 points)						
max-norm	<b>0.36 (0.16)</b>	<b>0.36</b>	<b>0.61 (0.14)</b>	<b>0.64</b>	<b>0.72 (0.14)</b>	<b>0.76</b>
l2-norm sq	0.35 (0.16)	0.35	0.61 (0.14)	0.63	0.72 (0.13)	0.74
l2-norm	0.35 (0.16)	0.35	0.61 (0.14)	0.63	0.72 (0.13)	0.74
l1-norm	0.34 (0.16)	0.34	0.60 (0.14)	0.62	0.71 (0.12)	0.73
sum,abs	0.32 (0.15)	0.32	0.57 (0.14)	0.59	0.71 (0.12)	0.73
sum,pos	0.24 (0.09)	0.24	0.40 (0.06)	0.41	0.71 (0.12)	0.73

**IG with zero baseline.** For the IG method, we tried several baseline images.

We obtained the best results when using as a baseline a constant image, where the pixel values are set to the mean channel values which we obtained over the flattened images of the CLEVR training data (these are the results we report in the main paper). We also tried using the mean image over the CLEVR training set images as a baseline, which gave us slightly inferior results to using the mean channel values.

Lastly, we tried using a zero-valued image as a baseline (as was done by the original authors [23]), the corresponding results can be found in Tables 7-8. With this baseline, IG performs very poorly, and on-par with GI. This illustrates the crucial importance of choosing a good IG baseline.

In our setup, using the mean channel values as a baseline led to the best results probably because all our images have the same grey background, which is uninformative for the prediction task. Furthermore, we did not preprocess the input images via centering (i.e. our images are in the range  $[0, 1]$ ).

**Table 7.** Relevance accuracy using the *mass metric* and a *single object* as ground truth, for different types of relevance pooling, and considering different data subsets. Here we report **IG with a zero baseline** (cf. Table 1 in the main paper, middle column)

Mass Metric Single Object GT	IG with zero baseline	
	mean (std)	median
- all correctly predicted (39027 points)		
max-norm	0.12 (0.09)	0.09
l2-norm sq	<b>0.26 (0.21)</b>	<b>0.19</b>
l2-norm	0.12 (0.09)	0.09
l1-norm	0.11 (0.09)	0.09
sum,abs	0.11 (0.09)	0.08
sum,pos	0.11 (0.09)	0.08
- correctly predicted with softmax probability > 0.9999 (29324 points)		
max-norm	0.12 (0.10)	0.10
l2-norm sq	<b>0.27 (0.21)</b>	<b>0.20</b>
l2-norm	0.12 (0.09)	0.09
l1-norm	0.12 (0.09)	0.09
sum,abs	0.12 (0.10)	0.09
sum,pos	0.12 (0.10)	0.09

**Table 8.** Relevance accuracy using the *rank metric* and a *single object* as ground truth, for different types of relevance pooling, and considering different data subsets. Here we report **IG with a zero baseline** (cf. Table 3 in the main paper, middle column)

Rank Metric Single Object GT	IG with zero baseline	
	mean (std)	median
- all correctly predicted (39027 points)		
max-norm	<b>0.27 (0.16)</b>	<b>0.26</b>
l2-norm sq	0.25 (0.15)	0.23
l2-norm	0.25 (0.15)	0.23
l1-norm	0.23 (0.15)	0.22
sum,abs	0.22 (0.14)	0.20
sum,pos	0.17 (0.09)	0.16
- correctly predicted with softmax probability > 0.9999 (29324 points)		
max-norm	<b>0.28 (0.15)</b>	<b>0.27</b>
l2-norm sq	0.26 (0.15)	0.24
l2-norm	0.26 (0.15)	0.24
l1-norm	0.24 (0.15)	0.22
sum,abs	0.23 (0.14)	0.21
sum,pos	0.17 (0.09)	0.17

## C Implementation details

**Model.** Here we provide details on the RN model architecture and training.

The CNN part of the network is made of 4 layers, each with the following structure: `conv`  $\rightarrow$  `relu`  $\rightarrow$  `batchnorm`. Each convolutional layer has 24 kernels of size  $3 \times 3$  and stride 2, and no padding.

The LSTM part of the network is a unidirectional LSTM with word embeddings of size 32, and a hidden layer of size 128.

The Relation Network part of the model is made of 4 fully-connected layers of size 256, each followed with ReLU activation, and a final element-wise summation layer.

The classifier part of the network contains 3 fully-connected layers, where the first two layers have size 256 and are followed by ReLU activation. Additionally, the second layer uses dropout ( $p = 0.5$ ). The output layer has size 28.

For preprocessing the questions, we removed punctuation and applied lower-casing, this leaves us with a vocabulary of size 80.

For preprocessing the images, we rescaled the pixel values to the range  $[0, 1]$ , and resized the images to the size  $128 \times 128$  (the original CLEVR images have size  $320 \times 480$ ).

Training was done with the Adam optimizer, using a batch size of 64, an initial learning rate of  $2.5e-4$ , clipping the gradient norm to 5.0, l2-norm regularization of  $4e-5$ , and decreasing the learning rate by a factor of 0.95 once the validation accuracy does not improve within 10 epochs. Training was done for a maximum of 1200 epochs.

During training, we also applied data augmentation (random cropping and random rotating of the images), as described in the original paper [20].

**Ground truth mask resizing.** Since the RN model architecture uses input images of size  $128 \times 128$ , the ground truth masks also have to be resized to this size.

For that purpose, we proceeded in the following way: we resized the masks using the same operation as for resizing the input images, starting with masks having a value of 1.0 on the ground truth pixels, and 0.0 elsewhere. Then, after resizing the masks, we set all pixels having a non-zero value to True, and the remaining pixels to False. This way we ensure that the resulting masks also include the objects' borders (which are slightly dilated by the resizing operation).